Surface Curvature Effects on the Tonal Noise Performance of a Low Reynolds Number Aerofoil

Xiang Shen[a], Eldad Avital[a], Qinghe Zhao[b], Junhui Gao[b], Xiaodong Li[b], Gordon Paul[a], Theodosios Korakianitis[c,*]

[a]*School of Engineering and Materials Science, Queen Mary University of London, London, E1 4NS, UK*
[b]*School of Jet Propulsion, Beihang University, Xueyuan Road 37, Beijing 100191, China*
[c]*Parks College of Engineering, Aviation and Technology, Saint Louis University, St. Louis, Missouri 63103, USA*

Abstract

This paper presents wind tunnel experiments to illustrate the effects of surface curvature on the aeroacoustic performance of airfoil E387. For the first time, surface curvature effects are considered in an investigation of the airfoil's self-noise. To distinguish the effects of surface curvature, the CIRCLE method is applied to the airfoil E387 to remove slope-of-curvature discontinuities and the redesigned airfoil is denoted A7. Anechoic wind tunnel tests were performed with E387 and A7 at three low Reynolds numbers to investigate aeroacoustic performance by measuring airfoil self-noise at different angles of attack (AoA) and spatial positions. At 2° and 4° AoA, A7 presents a tone with a reduced amplitude compared with E387 due to its improved slope-of-curvature distribution. It is concluded that improving surface curvature distribution improves airfoil aeroacoustic performance.

1. Introduction

At low Reynolds numbers the flow on an aerofoil separates due to a sufficiently large magnitude of the adverse pressure gradient and changes in flow geometry including local surface curvature variations. The flow experiences transition to turbulence and can result in a stall (without turbulent re-attachment) or a laminar separation bubble (with turbulent re-attachment) [1]. The turbulence produced in the boundary layer and near wake interacts with the aerofoil surface, producing aerofoil self-noise which contains tonal and broadband noise at low Reynolds numbers.

The mechanism of tonal noise has been researched since 1970s and it is often treated as a low Reynolds number phenomenon [2]. Most researchers [3–5] believe that this sound amplifying phenomenon occurs at certain frequencies via an acoustic feedback mechanism in the vicinity of the trailing edge. Sandberg et al. [6] suggested that the unsteady wake interacting with the trailing edge and pressure fluctuations due to vortex shedding are also responsible for the tonal noise generation, which is consistent with the category of Brooks et al. [7]. They also indicated that the aerofoil profile geometry affects the flow wake frequency. Desquesnes et al. [8] proposed a secondary feedback loop mechanism. They pointed out that the instabilities of boundary layer from suction side of the aerofoil are also important to the tone noise generation while the main tone

*Corresponding Author, Professor. Email forward for life: korakianitis@alum.mit.edu

noise frequency is decided by the boundary layer before the separation bubble along the pressure side. It has been found that for a symmetric aerofoil at zero angle of attack, the primary tonal noise amplitude decreases with the increasing of Reynolds number [9], the reasons why airfoils at low Reynolds numbers produce high levels of tonal noise still remains unclear.

It must be noted that the main attentions of the research works performed on the tonal noise mechanisms are paid on symmetric aerofoils, especially NACA0012. Little attention was paid to asymmetric aerofoils which also exhibit tonal noise phenomenon as will be presented in this paper. It should also be noticed that the experimental studies reviewed above may vary from each other depending on the testing conditions, e.g., the differences of turbulence intensity in the testing sections [10], the manufacturing precision of the testing aerofoil especially the surface finishing, etc. Although there are several different proposed mechanisms [5, 8, 9, 11, 12] regarding the generation of tonal noise, it is agreed that a necessary condition for acoustic tones is that the laminar separation bubble (LSB) is adequately close to the TE of the aerofoil, i.e., the position of laminar-turbulent transition must be sufficiently downstream so the large scales in the flow can be presented near the TE. This necessary condition has been used in the hypothesis of Jones et al. [13] on the feedback loop that can promote tonal noise in turbulent flows.

On the other hand, in terms of surface curvature effects, researchers have shown that aerofoil boundary layer behaviour can be improved by making the curvature distribution of an aerofoil continuous and smooth [14, 15]. The idea came originally from high-efficiency turbomachinery blade design, in which the distribution of surface curvature is an important factor [16, 17]. Massardo et al. [18, 19] used streamline curvature distribution calculations to determine the 3D variation of inlet and outlet flow angles for axial-flow compressor design and improved the compressor efficiency. Korakianitis et al. proposed a design method [20] to optimize aerofoils by ensuring continuous distributions of curvature and gradient-of-curvature along the surfaces, and showed that the aerodynamic and heat transfer performance strongly depended on curvature and gradient-of-curvature distribution. Based on surface curvature distribution, Song et al. [21] showed that continuous curvature distribution at the LE blending position of a compressor blade improves performance by helping to eliminate the separation bubble.

On low Reynolds number airfoils, researchers found that surface curvature and slope-of-curvature have impacts on the behaviour of the boundary layer on an airfoil by affecting the size of the laminar separation bubble (LSB). Korakianitis et al. [22] applied smooth curvature distributions to two wind turbine airfoils and numerically presented the aerodynamic improvements of the airfoils. Based on that, Shen et al. [23] expanded the work to three Reynolds numbers and a range of angles of attack, and they numerically [24] and experimentally [25] concluded that continuous surface curvature and slope-of-curvature distributions improved the aerodynamic performance through the effects on the laminar boundary layer including the LSB size contraction. These effects on the LSB size at low angles of attack have potential effects on the on airfoil acoustic performance in low Reynolds numbers, especially the tonal noise performance. Hence in this paper we experimentally examine the effects of slope-of-curvature on the aeroacoustic tonal noise performance of an airfoil.

The CIRCLE method [26] is used to redesign the airfoil by removing the slope of surface curvature

discontinuities from LE to TE. A typical low Reynolds number airfoil E387 is judiciously selected for the investigation due to the existence of discontinuities of slope-of-curvature, its widespread use and the availability of detailed experimental measurements of airfoil performance [27, 28]. The newly designed airfoil is denoted as "A7". Both airfoils are manufactured in Queen Mary University of London (QMUL). The anechoic wind tunnel experiments were carried out in Beihang University. The experimental results of two airfoils are compared to analyze the aeroacoustic performance differences caused by the different curvature distributions. These experimental measurements deepen our knowledge of the effects of slope-of-curvature discontinuities on the airfoil self-noise including tonal noise.

2. Redesign of the airfoil E387 with the CIRCLE Method

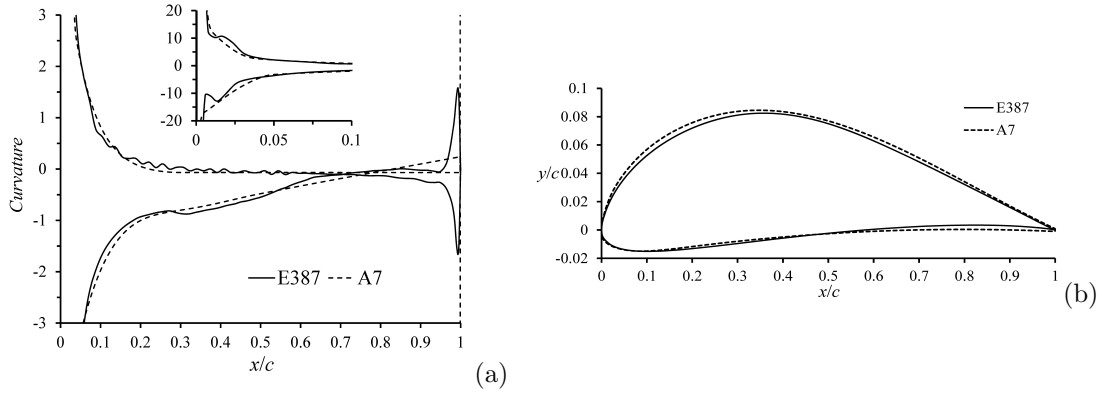

Figure 1: The comparison of (a) curvature distributions and (b) airfoil geometries of the original airfoil E387 [22] and redesigned airfoils A7. The subfigure in figure(a) is the magnification of the curvature distributions at the leading edge area.

Many airfoil geometries including E387 have discontinuities in surface slope-of-curvature distributions [26]. These discontinuities are observable as unsmooth "kinks" in airfoil curvature distributions. A smooth curvature distribution is equivalent to a continuous slope-of-curvature distribution. Based on this, the CIRCLE method, which was previously documented [26], is applied to the airfoil E387 to remove the discontinuities in slope-of-curvature distributions. The original and redesigned airfoils are presented in Figure 1. The curvature distributions are presented in Figure 1(a) and the geometries are compared in Figure 1(b). The curvature distributions are calculated from the definition of surface curvature, as shown in Eq. 1, and the definition of slope-of-curvature is presented in Eq. 2. The sign of the curvature is usually defined as the direction of the unit tangent vector moving along the curve. In order to clearly present the curvature distributions of both suction and pressure sides simultaneously, we define curvature as positive if the vector rotates clockwise (suction side) from the LE, otherwise it is negative (pressure side).

$$Curv = \frac{1}{r} = \frac{y''}{(1+y'^2)^{(3/2)}} \tag{1}$$

$$Curv' = \frac{d(Curv)}{dx} = \frac{y'''(1+y'^2) - 3y'y''^2}{(1+y'^2)^{(5/2)}} \tag{2}$$

In Figure 1(a) the unsmooth parts (slope-of-curvature discontinuities) including two obvious "kinks" in the magnified figure are exhibited on both sides of the airfoil E387, although most of the slope-of-curvature

discontinuities are in the suction surface. The airfoil A7 has a smooth curvature distribution without any slope-of-curvature discontinuities. The continuous slope-of-curvature distribution of A7 results in very slight differences in thickness and camber distributions.

3. Experimental Facility and Measurement Techniques

Anechoic wind tunnel measurements were performed to the original airfoil E387 and the redesigned airfoil A7 at chord-length based Reynolds number 100,000, 200,000 and 300,000 to investigate their aeroacoustic performance. The airfoil self-noise was measured at different angles of attack (AoAs) and different spatial positions.

3.1. Wind Tunnel Facility

This experimental study was conducted in the D5 subsonic wind tunnel with a $7m \times 6m \times 6m$ (L×W×H) anechoic chamber. It is a closed-circuit type tunnel with a 9:1 contraction ratio. An open testing section is applied for aeroacoustic measurement purpose, and the length of the open testing section is 2.5 m. The cross-section size of the testing section is $1m \times 1m$ (W×H). The wind speed in the test section can be increased up to 100 m/s, driven by a 210 kW AC motor and a 16-bladed fan with a $2.26m$ diameter.

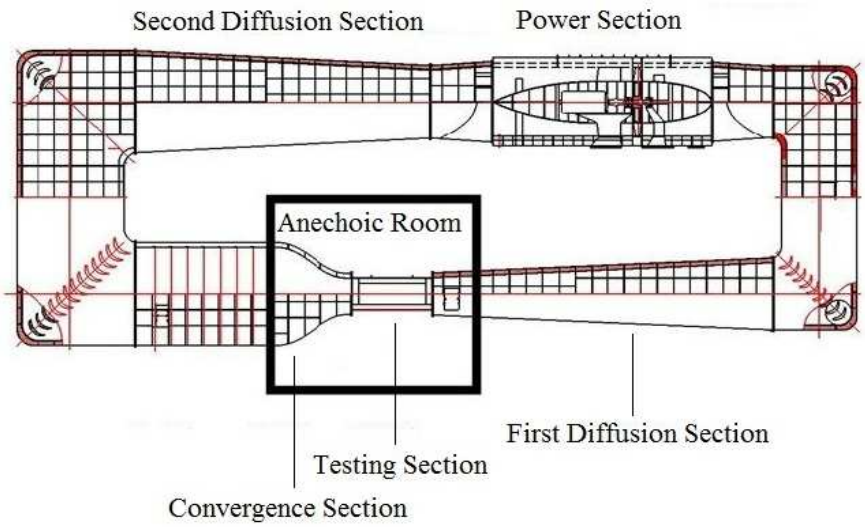

Figure 2: The schematic diagram of the D5 subsonic anechoic wind tunnel structure

The schematic layout of the wind tunnel structure is presented in Figure 2. The whole tunnel is located on the same floor. During the tests the flow originates from the power section and converges to the testing section. The flow subsequently passes through the first diffusion section, returns to the power section and recycles with new generated flow. The turbulence intensity that was measured at the centerline of the open testing section is found to be lower than 0.1% for all tests described in this paper.

3.2. Airfoil Models

Tests were separately conducted on two airfoil models. The chord length and span length of each model is 200 mm and 1000 mm respectively. The model is composed of five 200 mm sections, and each section

was manufactured from ABS M30 using a 3D printing process with a Stratasys Fortus 450mc 3D printer. This printer has an achievable accuracy of 0.127 mm (0.005 $inch$). The airfoil models were built with high precision.

Three studding rods are fixed through all five 200 mm sections with nuts at the end of the top section. Three 5 mm Dowel pins are used to connect each pair of neighboring sections. Each airfoil model is mounted vertically in the wind tunnel. The bottom of the airfoil model was fitted with a 30 cm diameter end-plate which is embedded and rotatable in the lower side of the square nozzle of the test section. One 8 mm dowel pin was used to connect the model top and the upper side of the square nozzle. It is an interference fit between the dowel pin and airfoil top, and a sliding fit between the dowel pin and the upper side of the square nozzle. In this way the angle of attack can be adjusted by rotating the scaled end-plate embedded in the lower side of the square nozzle. The pitching axis of the airfoil was located at the quarter-chord point which is a common approximate location of the aerodynamic center.

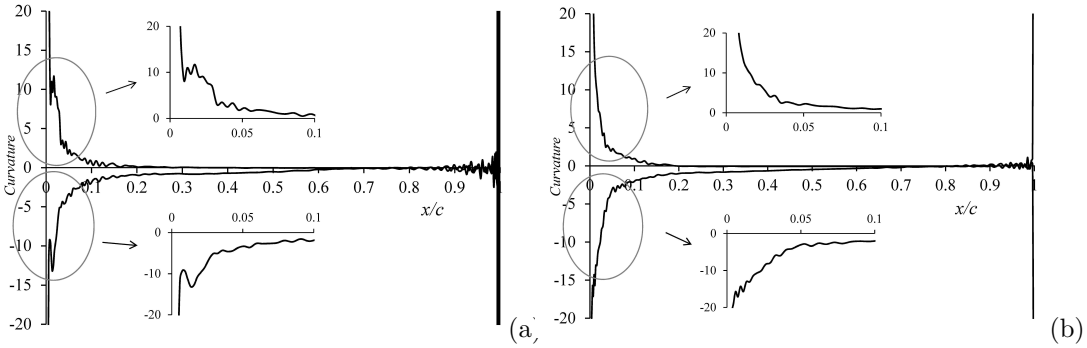

Figure 3: Curvature distributions of the 3D printed airfoils calculated from the measured coordinates of manufactured airfoil sections (a) E387 (b) A7. The small figures are magnifications of the circled parts of the graph.

No pressure measurement orifices are needed in the present aeroacoustic experiments. Hence the trailing edge (TE) thickness of the airfoil model E387 can be manufactured to the lower limit of the Stratasys Fortus machine, no greater than 0.13 mm. The designed surface curvature distributions of both airfoils are retained because no surface damaging actions such as drilling were applied to the models. The models were digitised using a QCT Quantum GL 6105 coordinate measuring machine (CMM) to determine the actual airfoil shape in order to determine the accuracy of the manufactured models. The surface curvature distributions of both airfoil are calculated from the measured coordinates, as presented in Figure 3. The high-precision manufacture preserved the slope-of-curvature discontinuities existing in the original design which is presented in Figure 1. The main differences between the curvatures are near LE and TE. The main body part of each airfoil keeps a smooth curvature distribution with a small magnitude. In Figure 3(a), the unsmooth curvature distributions of E387 at the connection part between the LE and the main body indicates that the manufactured airfoil model E387 successfully retains the slope-of-curvature discontinuities in the original design. The curvature distributions of A7 in Figure 3(b) show the removal of the slope-of-curvature discontinuities. The precision limit of airfoil manufacture and coordinate measurement introduced slight fluctuations to both curvature distributions. The difference between the designed and manufactured

surface was measured to be within 0.05% of the model chord length. Generally the two airfoils reproduced the design and met wind tunnel testing requirements.

3.3. Measurement Techniques and Data Acquisition

Acoustic pressure fluctuation data were acquired using B&K Type 4939 1/4-inch free-field microphones at different positions as shown in Figure 4. The positions were localised by a Stanley TLM99 Laser Distance Measurer with a ± 2 mm accuracy. The microphones were individually calibrated with a standard sound source B&K pistonphone Type 4228 which has a sound pressure level (SPL) of 124 ± 0.2 dB at 250 Hz calibration frequency.

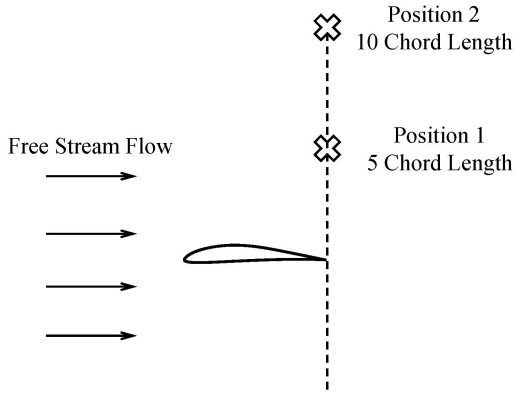

Figure 4: The schematic diagram of microphone positions in the anechoic chamber

Data acquisition and analysis was performed in a PC equipped with a data acquisition card NI PXI-4496 and was based on the commercial software LabView. The sampling frequency in the experiments is 16384 Hz, and the sampling time is 10 seconds.

No microphone directivity corrections were applied due to the negligible effect in the measurements (less than 1 dB for 45° offtrack [29]) and the effect is same for both airfoils. Relative humidity in air has a measurable effect on the air density, so we used the Shelquist's correction of air humidity [30] to correct air density in this chapter. However, the humidity in Beijing was less than 8% during the experiments, meaning it was close to the ideal dry air and the effects on the sound speed can be neglected [31]. Therefore no humidity corrections were made to the sound speed.

The SPL is made on a logarithmic scale due to the wide range of the sound, and it can be calculated from:

$$L_p = 20log_{10}(\frac{p}{p_0})\ dB \tag{3}$$

where L_p denotes SPL, p denotes the measured sound pressure fluctuations and p_0 denotes the reference sound pressure in air which commonly refers to the threshold of hearing: 2×10^{-5} Pa.

4. Results and Discussion

4.1. The effects of the angles of attack

At $Re = 10^5$ the broadband acoustic noise spectra of the noise levels for the airfoil E387 and A7 at $AoA = 2°$, $4°$ and $6°$ are presented in Figure 5. Three tonal noise peaks are observed for each airfoil. The primary tonal noise of E387 is found at 192 Hz and the SPL of the tone decreases as the AoA increases. At $AoA = 2°$ the SPL of the dominant tone of the airfoil E387 is 45 dB and it reduces to 38 dB when the AoA decreases to $4°$, while at $AoA = 6°$ the tonal noise peak is not observed at 192 Hz frequency. The primary tonal noise of A7 is observed at the frequency 176 Hz which is slightly lower than the dominant tone frequency on E387. For the airfoil A7 the SPL of the dominant tone is found to be 41 dB at $AoA = 2°$ which is approximately 10% lower than that on E387. At $AoA = 4°$ the primary tone on A7 becomes very weak and it presents as a narrowband noise in the vicinity of 176 Hz frequency. Similar to E387, the airfoil A7 does not present tonal noise peak at $AoA = 6°$.

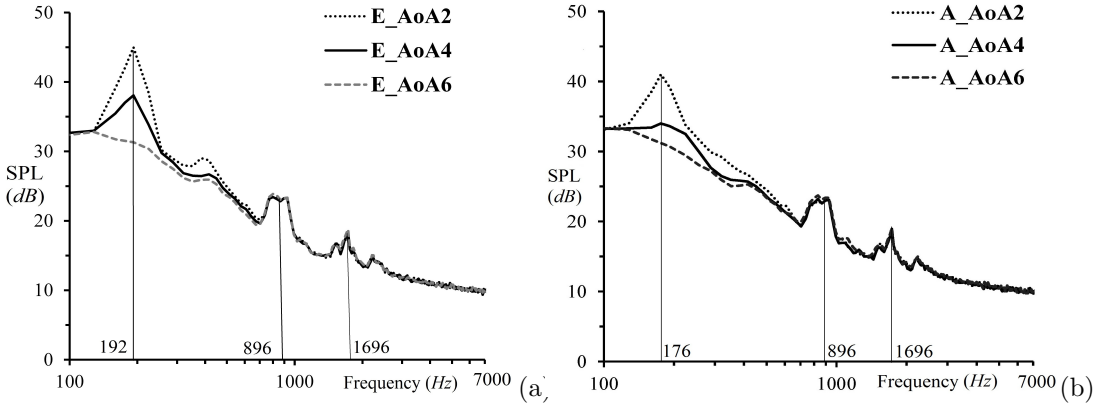

Figure 5: Acoustic noise spectra (integrated over 16 Hz bandwidth width) of the airfoil (a) E387 and (b) A7 at $AoA = 2°$, $4°$ and $6°$ at $Re = 10^5$. The results are obtained at position 1 in Figure 4.

However, for both airfoils the tonal peaks at 896 Hz and 1696 Hz barely vary with the different AoAs. It is suspected that these two peaks can be resulted from the background noise of testing section. For measuring purpose the testing section is an open type, hence the flow background noise is unavoidable when the flow is collected into the first diffusion section, as shown in Figure 2. We measured the background noise with no airfoil mounted in the testing section in order to compare with the current results and to identify the source of the two tonal peaks at 896 Hz and 1696 Hz. It must be noted that the empty tunnel noise spectra are not a absolutely true indication of the background noise with an airfoil installed, because the blockage that resulted from the airfoil model causes the fan of the wind tunnel to operate at a higher rotation speed. Nevertheless the noise spectra of the empty tunnel can clearly presents the broadband noise generated by the background noise, as shown in Figure 6.

Figure 6 also compared the SPL measured in two measurement positions. In Figure 6 (a), closer measuring position results in greater calculated SPL as well as sharper tones compared to Figure 6 (b). In both subfigures the tonal noise peaks at 896 Hz and 1696 Hz of the three acoustic noise spectra nearly overlap, indicating that these two tones actually result from the background noise, rather than from the airfoils.

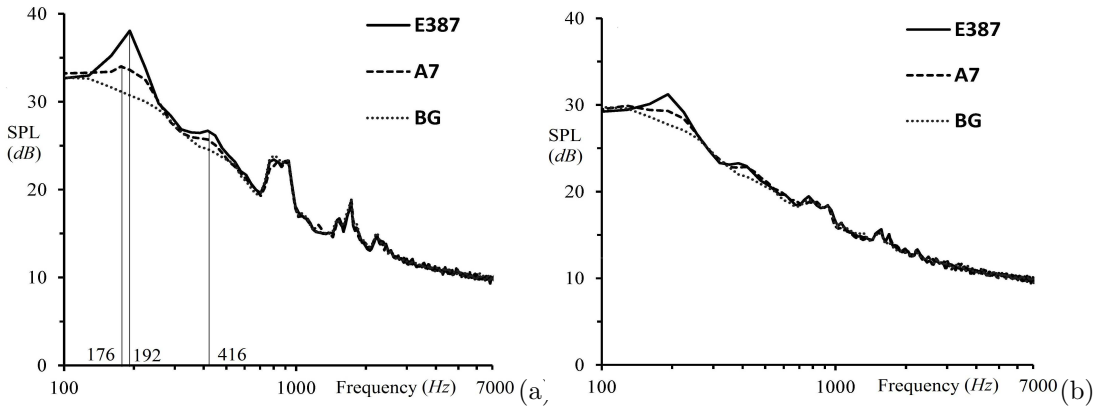

Figure 6: Acoustic noise spectra (integrated over 16 Hz bandwidth width) of the both airfoils and the empty tunnel at $AoA = 4°$ and $Re = 10^5$. The results are measured at (a) position 1 and (b) position 2 in Figure 4. BG denotes the background noise of the empty tunnel.

Yet the primary tone of E387 and A7 at 192 Hz and 176 Hz respectively presents distinct differences from the acoustic noise spectra of the background noise, and a secondary tone at 416 Hz for each airfoil, which acts as a higher harmonic, is detected with the reference of the background noise. Hence these tones are considered as the airfoils' self-noise tones in the current experimental work.

The broadband acoustic noise spectra in the 16 Hz bandwidth can clearly present the peaks in the frequency field. It can also clearly show the SPL distribution in the high frequency range because low frequency resolution introduces fewer SPL fluctuations, particularly when the frequency is greater than 1000 Hz. However, there are two disadvantages of the spectra of low frequency resolution which make the narrowband acoustic noise spectra necessary for the current case. One is that small peaks of the spectra can be neglected. The other is that the precision of the predicted frequency of the detected tones is low, so the corresponding frequency of the SPL peaks can be inaccurate due to the low frequency resolution. The inaccuracy usually presents as a small frequency offset depending on the bandwidth.

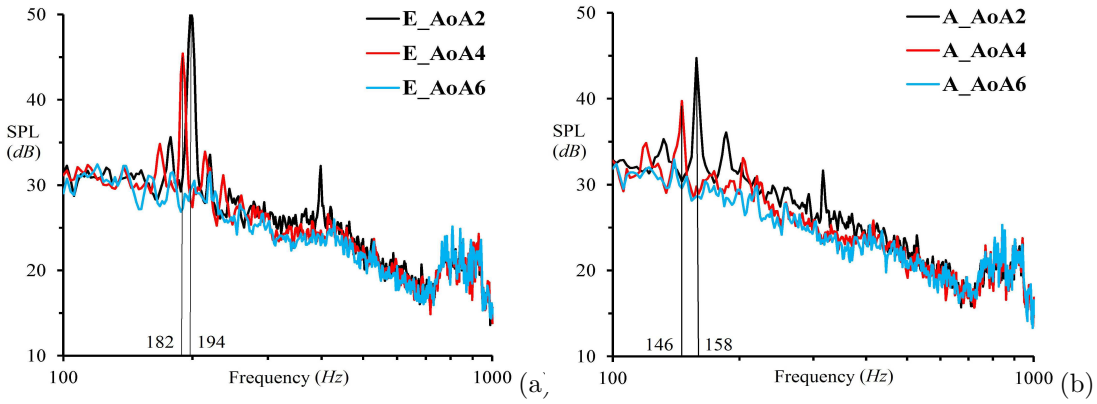

Figure 7: Acoustic noise spectra (integrated over 1 Hz bandwidth) of the airfoil (a) E387 and (b) A7 at $AoA = 2°$, 4° and 6° at $Re = 10^5$. The results are obtained at position 1 in Figure 4.

Corresponding to Figure 5, the narrowband acoustic noise spectra in the 1 Hz bandwidth is presented in Figure 7. Figure 7 (a) shows that the primary tonal frequencies of E387 at $AoA = 2°$ and $AoA = 4°$ are 194 Hz and 182 Hz respectively, with an offset of $+2$ Hz and -10 Hz compared to the acoustic noise spectra

in the 16 Hz bandwidth. The primary tone found at $AoA = 2°$ has the greatest SPL magnitude compared to the other two attack angles, and the SPL is greater than 50 dB. A secondary tone is observed at 398 Hz which appears as a higher harmonic. As the AoA increases to 4°, the SPL of the primary tone decreases by 6 dB and the frequency of the primary tone decreases by 8 Hz. No tonal noise was detected at $AoA = 6°$ which is consistent with the acoustic noise spectra observed with the 16 Hz bandwidth.

Figure 7 (b) shows that the primary tonal frequencies of A7 in $AoA = 2°$ and $AoA = 4°$ are 158 Hz and 146 Hz respectively, with an offset of -16 Hz and -30 Hz compared to the acoustic noise spectra observed with the 16 Hz bandwidth, which further confirmed the necessity of using the spectra of high frequency resolution. As previously described in the drawbacks of the low frequency resolution, The primary tone on A7 at $AoA = 4°$ can be easily ignored with the low frequency resolution (Figure 5 (b)), but is clearly observed with the high frequency resolution (Figure 7 (b)) due to the small bandwidth. The primary tone on A7 is, however, less significant than the dominant tone produced by E387 (Figure 7 (a)) in terms of amplitude. The primary tone found at $AoA = 2°$ has the greatest SPL magnitude among three angles of attack, and the SPL is 45 dB. As the AoA increases to 4°, the SPL of the primary tone decreases by 5 dB and the frequency of the primary tone decreases by 8 Hz. Consistent with the acoustic noise spectra in 16 Hz bandwidth, no tonal noise was detected at $AoA = 6°$.

The differences between the dominant tone frequency of E387 and A7 are both 36 Hz at $AoA = 2°$ and 4°. The offset of the dominant tone frequency between these two airfoils could be caused by the difference in the geometry of the trailing edge. In the research of Ramirez and Wolf [32], an airfoil shape was tested with four different TE bluntness, and it was found that thicker bluntness of the TE can result in a lower dominant tone frequency. This explains the presented offset of the dominant tone frequency between these two airfoils E387 and A7. The TE thickness of E387 is determined by the manufacturing precision because ideally the TE tapers towards zero thickness. At least one deposition layer is required for adequate structure strength so the manufactured TE thickness of E387 is 0.127 mm. The designed TE radius of airfoil A7 is 0.00105 chord length, leading to a manufactured TE thickness of 0.48 mm, which is almost 4 times the manufactured TE thickness of E387.

At $Re = 10^5$, the airfoil A7 presents lower SPL of the primary tonal noise comapred to E387 at $AoA = 2°$ and 4°, and the SPL magnitude is decreased by 7 dB and 5 dB respectively. These reductions are believed to result from the removal of the slope-of-curvature discontinuities because the two airfoils were manufactured with the same machine and they were tested in exactly same operating conditions. To investigate the mechanism of the reduction in dominant tonal noise, it is essential to understand the generation of the tonal noise. Although there are several different proposed mechanisms [5, 8, 9, 11, 12] regarding the generation of tonal noise, it is agreed that a necessary condition for acoustic tones is that the LSB is adequately close to the TE of the airfoil, i.e., the position of laminar-turbulent transition must be sufficiently downstream so the large scales in the flow can be presented near the TE. This necessary condition has been used in the hypothesis of Jones et al. [13] on the feedback loop that can promote tonal noise in turbulent flows. In the previous experimental [25] and numerical study [23, 24], it was observed that the size of the LSB on airfoil A7 is smaller and the position is more upstream compared to the bubble on E387 at 4° and $Re = 10^5$. This

correlates with the lower SPL of the primary tonal noise according to the necessary condition for acoustic tones. The process is similar to the LSB variation when increasing the AoA of an airfoil at the current Reynolds number. As the AoA increases at a constant Reynolds number, the LSB contracts and moves upstream , while the SPL of the primary tonal noise gets weaker as shown in Figure 5 and Figure 7. These observations provide strong evidence for a causal relationship between the LSB position and the SPL of the primary tone, as hypothesised by Nash et al. [5]. The removal of the slope-of-curvature discontinuities on airfoil E387 leads a smaller size of LSB to be more upstream, hence the airfoil tonal noise is reduced.

Hence the SPL spectra provided by the lower frequency resolution in Figure 5 is the preferred indicator if the broadband acoustic noise spectra are analysed globally without introducing unnecessary numerical noise, while the SPL acoustic noise spectra provided by the higher frequency resolution in Figure 7 is preferred if the narrowband acoustic noise spectra with particular details of tonal noise peaks are required to be analyzed.

4.2. The effects of Reynolds number

The broadband acoustic noise spectra for the airfoil E387 and A7 at $AoA = 4°$ and $Re = 1 \times 10^5$, 2×10^5 and 3×10^5 are presented in Figure 8. The low frequency resolution (16 Hz band width) is used because a broadband spectra is required to investigate the variation in the global trend when increasing the Reynolds number, and unnecessary numerical noise needs to be avoided to clearly identify the variation in tonal frequency.

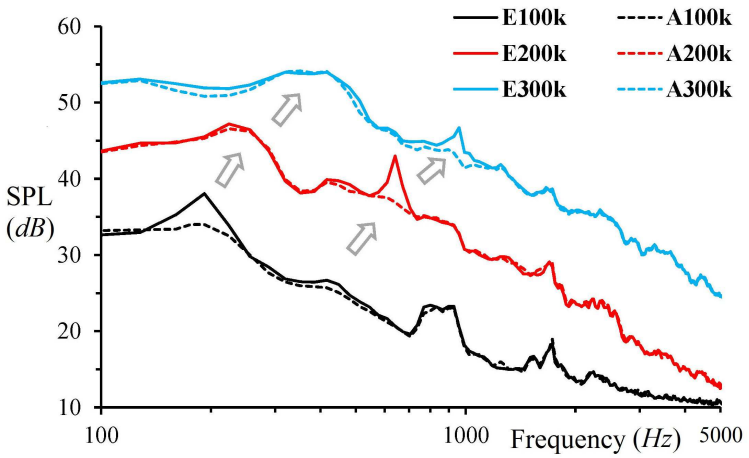

Figure 8: Broadband acoustic noise spectra (integrated over 16 Hz band width) of the noise levels for the airfoil E387 and A7 at different Reynolds numbers. The $AoA = 4°$ and $Re = 10^5$. The results are obtained at position 1 in Figure 4.

The SPL increases with Reynolds number, and the magnitude increases by approximately 10 dB when the Reynolds number increases by 10^5. The primary tonal frequency at $Re = 1 \times 10^5$ is no longer dominant at $Re = 2 \times 10^5$ or more. When increasing the Reynolds number, the secondary tone at $Re = 1 \times 10^5$ which was observed at 416 Hz in Figure 6 promotes to be the primary tonal frequency at $Re = 2 \times 10^5$ and this primary tone becomes weaker at $Re = 3 \times 10^5$. The phenomenon is a typical "Ladder-Structure" described in the study by Paterson et al. [11]. It indicates that at $Re = 2 \times 10^5$ and 3×10^5, as the flow

velocity is increased, the dominant tonal frequency is observed to follow a curve that approximates a $U^{0.8}$ dependence where U is the freestream velocity, while at $Re = 1 \times 10^5$ the dominant tonal frequency jumps to another parallel curve with the same $U^{0.8}$ dependence according to Paterson et al. [11]. At all three Reynolds numbers the airfoil A7 shows reduced SPL of the primary tonal noise.

5. Concluding Remarks

In this paper the effects of surface slope-of-curvature distributions on airfoil tonal noise are investigated. This has not been investigated previously to the best of the authors' knowledge. An anechoic wind tunnel experimental study is performed on airfoils E387 and A7 to investigate their self-noise performance at low Reynolds numbers. Three AoAs are considered in the experiment and for both airfoils tonal phenomena are observed at $AoA = 2°$ and $4°$, while no tonal noise is observed at $AoA = 6°$. It is found that the position of the LSB on the airfoil correlates with the SPL amplitude of the primary tonal noise according to the necessary condition for acoustic tones. At these two AoAs the airfoil tonal noise on A7 is reduced due to a smaller size of LSB to be more upstream, resulting from the removal of the slope-of-curvature discontinuities on airfoil E387. The slope-of-curvature discontinuities resulted in a tonal noise with an amplitude 13% greater on E387 compared to the airfoil A7 at $AoA = 2°$ and $4°$. The corresponding frequency of the primary tone on A7 is found to be 32 Hz lower than that on E387. It is concluded that continuous slope-of-curvature distributions improve the tonal noise performance of the low Reynolds number airfoils.

Acknowledgments

The support of the UK turbulence consortium for providing national computing time under Grant No. EP/L000261/1 was acknowledged. The authors acknowledge the Royal Society (Grant No. IE131709) and NFSC (Grant No. NFSC-5141130130, 51376015 and 51476005) that funded the visit to Beihang D5 wind tunnel and the production of the models. The PhD research of Xiang Shen is funded by China Scholarship Council (CSC)/ Queen Mary Joint PhD scholarship and is supervised by Theodosios Korakianitis and Eldad Avital.

References

[1] N. D. Sandham. Transitional separation bubbles and unsteady aspects of aerofoil stall. *Aeronautical Journal*, 112(1133):395–404, 2008.

[2] E Arcondoulis, CJ Doolan, AC Zander, and LA Brooks. A review of trailing edge noise generated by airfoils at low to moderate reynolds number. *Acoustics Australia*, 38(3):129–133, 2010.

[3] T Nakano, N Fujisawa, and S Lee. Measurement of tonal-noise characteristics and periodic flow structure around naca0018 airfoil. *Experiments in Fluids*, 40(3):482–490, 2006.

[4] Michael J Kingan and John R Pearse. Laminar boundary layer instability noise produced by an aerofoil. *Journal of Sound and Vibration*, 322(4):808–828, 2009.

[5] Emma C Nash, Martin V Lowson, and Alan McAlpine. Boundary-layer instability noise on aerofoils. *Journal of Fluid Mechanics*, 382:27–61, 1999.

[6] RD Sandberg, LE Jones, ND Sandham, and PF Joseph. Direct numerical simulations of tonal noise generated by laminar flow past airfoils. *Journal of Sound and Vibration*, 320(4):838–858, 2009.

[7] Thomas F Brooks, D Stuart Pope, and Michael A Marcolini. *Airfoil self-noise and prediction*, volume 1218. National Aeronautics and Space Administration, Office of Management, Scientific and Technical Information Division, 1989.

[8] G Desquesnes, M Terracol, and P Sagaut. Numerical investigation of the tone noise mechanism over laminar airfoils. *Journal of Fluid Mechanics*, 591:155–182, 2007.

[9] H Arbey and J Bataille. Noise generated by airfoil profiles placed in a uniform laminar flow. *Journal of Fluid Mechanics*, 134:33–47, 1983.

[10] John Stack. Tests in the variable density wind tunnel to investigate the effects of scale and turbulence on airfoil characteristics. Technical Report Technical Note 364, NACA, 1931.

[11] Robert W Paterson, Paul G Vogt, Martin R Fink, and C Lee Munch. Vortex noise of isolated airfoils. *Journal of Aircraft*, 10(5):296–302, 1973.

[12] Christopher KW Tam. Discrete tones of isolated airfoils. *The Journal of the Acoustical Society of America*, 55(6):1173–1177, 1974.

[13] Lloyd E Jones and Richard D Sandberg. Numerical analysis of tonal airfoil self-noise and acoustic feedback-loops. *Journal of Sound and Vibration*, 330(25):6137–6152, 2011.

[14] I. A. Hamakhan and T. Korakianitis. Aerodynamic performance effects of leading-edge geometry in gas-turbine blades. *Applied Energy*, 87(5):1591–1601, 2010.

[15] Y. Song and C. W. Gu. Effects of curvature continuity of compressor blade profiles on their performances. In *ASME Turbo Expo 2014: Turbine Technical Conference and Exposition*, pages V02AT37A020–V02AT37A020. American Society of Mechanical Engineers, 2014.

[16] T. Korakianitis. Design of airfoils and cascades of airfoils. *AIAA Journal*, Vol.27(4):455–461, April 1989.

[17] T. Korakianitis. Prescribed-curvature distribution airfoils for the preliminary geometric design of axial turbomachinery cascades. *Journal of Turbomachinery, Transactions of the ASME*, 115(2):325–333, April 1993.

[18] A. Massardo, A. Satta, and M. Marini. Axial Flow Compressor Design Optimization: Part II Throughflow Analysis. *Journal of Turbomachinery*, 112(3):405–410, 1990.

[19] AF Massardo and M Scialo. Thermoeconomic analysis of gas turbine based cycles. *Journal of engineering for gas turbines and power*, 122(4):664–671, 2000.

[20] T. Korakianitis, I. A. Hamakhan, M. A. Rezaienia, A. P. S. Wheeler, E. J. Avital, and J. J. R. Williams. Design of high-efficiency turbomachinery blades for energy conversion devices with the three-dimensional prescribed surface curvature distribution blade design (CIRCLE) method. *Applied Energy*, 89(1):215–227, 2012.

[21] Y. Song, C. W. Gu, and Y. B. Xiao. Numerical and theoretical investigations concerning the continuous-surface-curvature effect in compressor blades. *Energies*, 7(12):8150–8177, 2014.

[22] T. Korakianitis, M. A. Rezaienia, I. A. Hamakhan, E. J. Avital, and J. J. R. Williams. Aerodynamic improvements of wind-turbine airfoil geometries with the prescribed surface curvature distribution blade design (CIRCLE) method. *Journal of Engineering for Gas Turbines and Power*, 134(8), 2012.

[23] X. Shen, T. Korakianitis, and E. J. Avital. Numerical investigation of surface curvature effects on aerofoil aerodynamic performance. *Applied Mechanics and Materials*, 798:589–595, 2015.

[24] Xiang Shen, Eldad Avital, Gordon Paul, Mohammad Amin Rezaienia, and T. Korakianitis. Computational methods for investigation of surface curvature effects on airfoil boundary layer behavior. *Journal of Algorithms & Computational Technology*, 11(1):68–82, 2017.

[25] Xiang Shen, Eldad Avital, Gordon Paul, Mohammad Amin Rezaienia, P Wen, and T. Korakianitis. Experimental study of surface curvature effects on aerodynamic performance of a low reynolds number airfoil for use in small wind turbines. *Journal of Renewable and Sustainable Energy*, 8:053303, 2016.

[26] T. Korakianitis, M.A. Rezaienia, I.A. Hamakhan, and A.P.S. Wheeler. Two- and three-dimensional prescribed surface curvature distribution blade design (CIRCLE) method for the design of high efficiency turbines, compressors, and isolated airfoils. *Journal of Turbomachinery*, 135(3), 2013.

[27] R. Mcghee, B. Walker, and B. Millard. Experimental results for the Eppler 387 airfoil at low Reynolds numbers in the Langley low-turbulence pressure tunnel. Technical report, NASA, 1988.

[28] M. S. Selig and B. D. McGranahan. Wind tunnel aerodynamic tests of six airfoils for use on small wind turbines. *Journal of solar energy engineering*, 126(4):986–1001, 2004.

[29] Paul Migliore and Stefan Oerlemans. Wind tunnel aeroacoustic tests of six airfoils for use on small wind turbines. *Journal of Solar Energy Engineering*, 126(4):974–985, 2004.

[30] Richard Shelquist. An introduction to air density and density altitude calculations. *Internet Survey*, 2012.

[31] Dennis A Bohn. Environmental effects on the speed of sound. *Journal of the Audio Engineering Society*, 36(4):223–231, 1988.

[32] Walter Arias Ramírez and William Roberto Wolf. Effects of trailing edge bluntness on airfoil tonal noise at low reynolds numbers. *Journal of the Brazilian Society of Mechanical Sciences and Engineering*, pages 1–12, 2015.